

# Probabilities of rapidity gaps in high energy interactions

A.B. Kaidalov<sup>1,2</sup>, V.A. Khoze<sup>1</sup>, A.D. Martin<sup>1</sup>, M.G. Ryskin<sup>1,3</sup>

<sup>1</sup> Department of Physics and Institute for Particle Physics Phenomenology, University of Durham, Durham, DH1 3LE, UK

<sup>2</sup> The Institute for Theoretical and Experimental Physics (ITEP), 117259 Moscow, Russia

<sup>3</sup> Petersburg Nuclear Physics Institute, Gatchina, St. Petersburg, 188300, Russia

Received: 16 May 2001 / Revised version: 12 July 2001 /

Published online: 10 August 2001 – © Springer-Verlag / Società Italiana di Fisica 2001

**Abstract.** We show that high energy hadronic reactions which contain a rapidity gap and a hard subprocess have a specific dependence on the kinematic variables, which results in a characteristic behaviour of the survival probability of the gap. We incorporate this mechanism in a two-channel eikonal model to make an essentially parameter-free estimate of diffractive dijet production at the Tevatron, given the diffractive structure functions measured at HERA. The estimates are in surprising agreement with the measurements of the CDF collaboration. We briefly discuss the application of the model to other hard processes with rapidity gaps.

## 1 Introduction

There has been much interest in the probability of rapidity gaps in high energy interactions to survive, since they may be populated by secondary particles generated by rescattering processes, see, for example, [1]– [8]. The effect can be described in terms of screening or absorptive corrections. To the best of our knowledge, the term survival probability was introduced by Bjorken [2] who estimated the probability using

$$S^2 = \frac{\int |\mathcal{M}(s, b)|^2 e^{-\Omega(b)} d^2b}{\int |\mathcal{M}(s, b)|^2 d^2b}, \quad (1)$$

where  $\mathcal{M}$  is the amplitude (in impact parameter  $b$  space) of the particular process of interest at centre-of-mass energy  $\sqrt{s}$ .  $\Omega$  is the opacity (or optical density) of the interaction of the incoming hadrons<sup>1</sup>.

It is perhaps more accurate to use the term “suppression factor” of a hard process accompanied by a rapidity gap, rather than “survival probability”. It depends not only on the probability of the initial state to survive, but is sensitive to the spatial distribution of partons inside the incoming hadrons, and thus on the dynamics of the whole diffractive part of the scattering matrix. It is important to note that the suppression factor  $S^2$  is not universal, but depends on the particular hard subprocess, as well as the kinematical configurations. In particular,  $S^2$  depends on the nature of the colour-singlet (Pomeron or  $W/Z$  boson or photon) exchange which generates the gap as well as

on the distributions of partons inside the proton in impact parameter space [9–12]. In this paper we emphasize the importance of the dependence on the characteristic momentum fractions carried by the active partons in the colliding hadrons. This leads to a much richer structure of the probability of rapidity gaps in processes mediated by colour-singlet  $t$ -channel exchange. The framework was introduced long ago<sup>2</sup> [15,16], but only with the advent of rapidity gap events being observed in hard processes at the Tevatron and at HERA, is this rich physics now revealing itself.

In Sect. 2 we briefly review the general framework, and, in particular, discuss a two-channel partonic model of diffraction. Measurements of diffractive dijet production with a leading antiproton have been made recently by the CDF collaboration [17] at the Tevatron. This is an ideal process with which to compare the specific predictions of the models for high energy diffraction. In Sect. 3 we specify the partonic structure of the diffractive two-channel eigenstates. To set the scene for our main study we first, in Sect. 4, discuss diffractive dijet production assuming, for the moment, that rescattering corrections may be neglected. As was emphasised in [17], the calculation of the cross section, based on factorization in terms of diffractive structure functions obtained from HERA data, indicates a large discrepancy with the CDF measurements – both in the normalisation and in the shape of the observed distribution. The calculation lies about a factor of 10 above the data; the precise discrepancy depends on the kinematic domain. In Sect. 5 we include rescattering corrections. Clearly these will decrease the predictions, since now the rapidity gaps may be populated by secondary

<sup>1</sup> That is  $i[1 - \exp(-\Omega/2)]$  is the usual elastic scattering amplitude in impact parameter space.  $\Omega/2$  is frequently called the eikonal.

<sup>2</sup> Reviews can be found, for example, in [13,14].

particles. To allow for rescattering we use the two-channel eikonal model, reviewed in Sects. 2 and 3, with parameters previously determined in a global description of the total, elastic and soft diffractive data available in the ISR to Tevatron energy range [9]. In this way we are able to make an essentially parameter-free prediction of both the normalisation and the shape of the CDF diffractive dijet data. In Sect. 6 we discuss the application of the model to other hard processes with rapidity gaps, but on a less quantitative level than for dijet production. In all cases the specific rescattering corrections are in the direction to improve the description of the data. Finally, in Sect. 7, we present our conclusions.

## 2 Inelastic diffraction and diffractive eigenstates

In order to deduce the behaviour of inelastic diffraction, we start with the  $s$ -channel unitarity relation, which interrelates the proton-proton total cross section, elastic and inelastic scattering. The unitarity relation is, in fact, valid at each value of the impact parameter separately, that is

$$2\text{Im} T_{fi} = \sum_n T_{nf}^* T_{ni}, \quad (2)$$

where  $T_{fi}(s, b)$  is the transition amplitude to go from state  $i$  to state  $f$ .

We follow a presentation by Pumplin [14], after the original interpretation of Good and Walker [15]. First we introduce states  $\phi_k$  which diagonalize the diffractive part of the  $T$  matrix. Such eigenstates of diffraction only undergo elastic scattering. Let us denote the orthogonal matrix which diagonalizes  $\text{Im} T$  by  $C$ , so that

$$\text{Im} T = CFC^T \quad \text{with} \quad \langle \phi_k | F | \phi_j \rangle = F_j \delta_{jk}. \quad (3)$$

Now consider the diffractive dissociation of an arbitrary incoming state

$$|i\rangle = \sum_k C_{ik} |\phi_k\rangle. \quad (4)$$

The elastic scattering amplitude for this state satisfies

$$\langle i | \text{Im} T | i \rangle = \sum_k |C_{ik}|^2 F_k = \langle F \rangle, \quad (5)$$

where  $F_k \equiv \langle \phi_k | F | \phi_k \rangle$  and where the brackets of  $\langle F \rangle$  mean the average of  $F$  over the initial probability distribution of diffractive eigenstates. After the diffractive scattering described by  $T_{fi}$ , the final state  $|f\rangle$  will, in general, be a different superposition of eigenstates than those of  $|i\rangle$  shown in (4). Suppose for simplicity, we neglect the real parts of the diffractive amplitudes, then

$$\frac{d\sigma_{\text{tot}}}{d^2b} = 2 \text{Im} \langle i | T | i \rangle = 2 \sum_k |C_{ik}|^2 F_k = 2 \langle F \rangle$$

$$\begin{aligned} \frac{d\sigma_{\text{el}}}{d^2b} &= |\langle i | T | i \rangle|^2 = \left( \sum_k |C_{ik}|^2 F_k \right)^2 = \langle F \rangle^2 \\ \frac{d\sigma_{\text{el} + \text{SD}}}{d^2b} &= \sum_k |\langle \phi_k | T | i \rangle|^2 = \sum_k |C_{ik}|^2 F_k^2 \\ &= \langle F^2 \rangle. \end{aligned} \quad (6)$$

It follows that the cross section for the single diffractive dissociation of a proton,

$$\frac{d\sigma_{\text{SD}}}{d^2b} = \langle F^2 \rangle - \langle F \rangle^2, \quad (7)$$

is given by the statistical dispersion in the absorption probabilities of the diffractive eigenstates.

Note that if all the components  $\phi_k$  of the incoming diffractive state  $|i\rangle$  were absorbed equally then the diffracted superposition would be proportional to the incident one and again the inelastic diffraction would be zero. Thus if, at very high energies, the amplitudes  $F_k$  at small impact parameters are equal to the black disk limit,  $F_k = 1$ , then diffractive production will be equal to zero in this impact parameter domain and so will only occur in the peripheral  $b$  region. This behaviour has already occurred in  $pp$  (and  $p\bar{p}$ ) interactions at Tevatron energies. On the other hand, if there are, say, two diffractive channels with different eigenvalues, then the amount of inelastic diffraction increases with the spacing of the two eigenvalues.

For instance, consider just two diffractive channels [18, 12, 9] (say,  $p, N^*$ ), and assume, for simplicity, that the elastic scattering amplitudes for the two channels are equal. Then the  $T$  matrix has the form

$$\text{Im} T = 1 - e^{-\Omega/2}, \quad (8)$$

where the eikonal matrix  $\Omega$  has elements

$$\Omega_{f'i'}^{fi} = \Omega_0 \omega^{fi} \omega_{f'i'}. \quad (9)$$

The individual  $\omega$  matrices, which correspond to transitions from the two incoming hadrons, each have the form

$$\omega = \begin{pmatrix} 1 & \gamma \\ \gamma & 1 \end{pmatrix}. \quad (10)$$

The parameter  $\gamma(s, b)$  determines the ratio of the inelastic to elastic transitions. The overall coupling  $\Omega_0$  is also a function of the energy  $\sqrt{s}$  and the impact parameter  $b$ .

With the above form of  $\omega$ , the diffractive eigenstates are

$$|\phi_1\rangle = \frac{1}{\sqrt{2}} (|p\rangle + |N^*\rangle), \quad |\phi_2\rangle = \frac{1}{\sqrt{2}} (|p\rangle - |N^*\rangle). \quad (11)$$

In this basis, the eikonal has the diagonal form

$$\Omega_{m'n'}^{mn} = \Omega_0 r^{mn} r_{m'n'}, \quad (12)$$

where  $m, n = \phi_1, \phi_2$  and

$$r = \begin{pmatrix} 1 + \gamma & 0 \\ 0 & 1 - \gamma \end{pmatrix}. \quad (13)$$

In the case where  $\gamma$  is close to unity,  $\gamma = 1 - \varepsilon$ , one of the eigenvalues is small.

### 3 Parton configurations of the diffractive eigenstates

The simple two-channel model of Sect. 2 allows the prominent features of hard diffractive processes to be explained, which are beyond the scope of the single channel eikonal. First we note that the parameter  $\gamma$ , which determines the ratio of inelastic to elastic transitions, needs to be in the range 0.4–0.6 to be in accord with the experimental data on diffractive dissociation at moderate energies. Thus we know that there will be a big difference ( $1 \pm \gamma$ ) in the absorptive cross sections for scattering in the two diffractive eigenstates. To be specific, in this work we use the results of the detailed analysis of the elastic and soft diffractive data that was presented in [9,10]. There  $\gamma$  was taken to be 0.4.

In QCD the diagonal states correspond to quark and gluon configurations with different transverse coordinates<sup>3</sup>. For small transverse size  $r$  such (colourless) configurations interact as small colour dipoles with total interaction cross sections  $\sim r^2$ . Thus, to a rough approximation, we can separate all the parton configurations of the colliding hadrons into those with small size and those with large size. In our two-channel example above these would correspond to the states  $|\phi_2\rangle$  and  $|\phi_1\rangle$  respectively.

It is informative to discuss the phenomenon in terms of the usual Reggeon diagrams. Assume that some “hard” diffractively produced state<sup>4</sup> “ $h$ ” is strongly coupled to state  $|\phi_2\rangle$  and weakly to  $|\phi_1\rangle$ . It follows from (11) that the Pomeron couplings of  $h$  to  $p$  and  $N^*$  satisfy

$$g_{ph}^{\mathbb{P}} = -g_{N^*h}^{\mathbb{P}}, \quad (14)$$

and that the  $p$  and  $N^*$  intermediate states for double-Pomeron exchange contribution (Fig. 1) interfere destructively, since

$$g_{pp}^{\mathbb{P}} g_{ph}^{\mathbb{P}} + g_{pN^*}^{\mathbb{P}} g_{N^*h}^{\mathbb{P}} = g_{pp}^{\mathbb{P}} g_{ph}^{\mathbb{P}} (1 - \gamma). \quad (15)$$

The cancellation which occurs for  $\gamma \approx 1$ , happens, in this simple model, for all multiple-Pomeron exchanges. This phenomenon of “colour transparency” for small-size configurations has been known for a long time [21].

In order to specify the diffractive eigenstates  $|\phi_1\rangle$  and  $|\phi_2\rangle$  we shall consider two simple models (A and B). It is natural to identify the component with the smaller absorptive cross section (that is  $|\phi_2\rangle$ ) with the state which contains less partons and which has a large typical momentum fraction  $x$  for each parton. From the QCD viewpoint, the small size component of the proton (where all

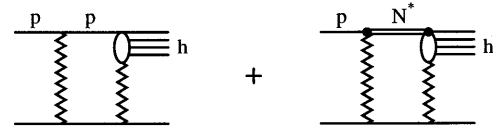


**Fig. 1.** The double-Pomeron exchange contribution to diffractive  $h$  production in the simple two-channel model of (13)

the valence quarks are close together) has the smallest absorptive cross section, due to colour transparency. From the Regge viewpoint, the component with the largest absorptive cross section corresponds to the eigenstate ( $|\phi_1\rangle$ ) with a larger number of partons in the small  $x$  region. Thus from both viewpoints we expect the component with the smaller cross section (smaller transverse size) to have a larger average  $x$  of each parton. At the moment, it is impossible to be more specific, and so to make numerical estimates we consider two alternatives.

First, in model A, we identify the valence quarks with  $|\phi_2\rangle$  with the smaller absorption, and the gluons and sea quarks with  $|\phi_1\rangle$ . Of course the model is oversimplified. It is clear that there is a part of the valence component with large size, while on the other hand the gluons and sea quarks contribute to the small size component. In general, one can write each partonic distribution  $f_i(x, Q^2)$  ( $i$  = valence, sea, glue) as the sum of a small ( $S$ ) and large ( $L$ ) size component

$$f_i(x, Q^2) = f_i^S(x, Q^2) + f_i^L(x, Q^2). \quad (16)$$

In a model, where the probabilities of the  $S$  and  $L$  components in the proton are equal, as in Sect. 2, these components should satisfy the following sum rules,

$$\begin{aligned} \int_0^1 dx f_V^S(x, Q^2) &= \int_0^1 dx f_V^L(x, Q^2) = \frac{3}{2} \quad (17) \\ \int_0^1 dx x \sum_i f_i^S(x, Q^2) &= \int_0^1 dx x \sum_i f_i^L(x, Q^2) \\ &= \frac{1}{2}, \quad (18) \end{aligned}$$

which follow from the conservation of valence quark number and energy respectively.

We can therefore introduce an alternative model in terms of modified parton distributions

$$f_i^{S,L}(x, Q^2) = P_i^{S,L}(x, Q^2) f_i(x, Q^2), \quad (19)$$

where the projection operators have the simple forms

$$P_i^L = (1 - x)^{n_i(Q^2)}, \quad P_i^S = 1 - P_i^L. \quad (20)$$

We determine the values of  $n_i$  in order to satisfy the sum rules of (17) and (18). We call this model B. It turns out that both models A and B give rather similar predictions. We study the implications of the models in Sect. 5.

### 4 Diffractive dijet production – a first look

Recently CDF have measured diffractive dijet production for events with a leading antiproton at the Tevatron [17].

<sup>3</sup> Partonic models of diffraction were originally introduced in [19,20].

<sup>4</sup> The state  $h$  should really be regarded as a third diffractive channel, but such a new state with a small production cross section gives a negligible contribution to  $\Omega$ .

These observations, coupled with the diffractive measurements by H1 [22] and ZEUS [23] at HERA, offer the opportunity to explore the diffractive framework in some detail. The processes are shown schematically in Fig. 2, in the absence of rescattering corrections. The lower parts of the diagrams, shown as Pomeron exchange, are to be understood as including multiple Pomeron contributions.

If we ignore rescattering corrections, for the moment, then the cross section for diffractive dijet production of Fig. 2a, integrated over  $t$ , may be written as

$$\sigma = \sum_{i,k} \int F_{\mathbb{P}}(\xi) f_i^{\mathbb{P}}(\beta, E_T^2) f_k^p(x_1, E_T^2) \hat{\sigma} d\beta dx_1 d\xi, \quad (21)$$

where  $\hat{\sigma}$  is the cross section to produce dijets from partons carrying longitudinal momentum fractions  $x_1$  and  $\beta$  of the proton and Pomeron respectively. This would correspond to the Ingelman-Schlein conjecture [24]. Information on the diffractive structure functions  $f_i^{\mathbb{P}}(\beta, Q^2)$  is obtained from measurements of the process of Fig. 2b at HERA [22,23].  $F_{\mathbb{P}}(\xi)$  is the flux factor taken for the Pomeron

$$F_{\mathbb{P}}(\xi) = \int dt \frac{C_{\mathbb{P}} e^{Bt}}{\xi^{2\alpha_{\mathbb{P}}(t)-1}}, \quad (22)$$

where  $\xi$  is the fractional momentum loss of the recoil antiproton. In Regge theory, the coupling satisfies  $C_{\mathbb{P}} = (g_{p\mathbb{P}}^{\mathbb{P}})^2/16\pi$ , such that the total  $p\bar{p}$  cross section is given by

$$\sigma_{\text{tot}}(p\bar{p}) = (g_{p\mathbb{P}}^{\mathbb{P}})^2 (s/s_0)^{\Delta}, \quad (23)$$

where  $s_0 \equiv 1 \text{ GeV}^2$  and  $\Delta = \alpha_{\mathbb{P}}(0) - 1$ . When  $\xi$  is not too small the contribution of secondary Reggeons must be added.

CDF present measurements of the ratio of dijet production for  $E_T(\text{jet1}, \text{jet2}) > 7 \text{ GeV}$  with a rapidity gap to that without a gap as a function of  $x = \beta\xi$  (the fractional longitudinal momentum of the  $\bar{p}$  carried by the parton), for six  $\xi$  bins in the range  $0.035 < \xi < 0.095$  with  $|t| < 1 \text{ GeV}^2$  [17]. In the ratio, the terms  $f_j^p(x_1, E_T^2)\hat{\sigma}$  cancel, assuming that single gluon  $t$ -channel exchange dominates the hard subprocess. Hence the data determine the diffractive structure function of the antiproton<sup>5</sup>

$$\begin{aligned} \tilde{F}_{jj}^D &= \frac{1}{\xi_{\text{max}} - \xi_{\text{min}}} \int_{\xi_{\text{min}}}^{\xi_{\text{max}}} d\xi F_{\mathbb{P}}(\xi) \beta \\ &\times [f_g^{\mathbb{P}}(\beta, E_T^2) + \frac{4}{9} f_q^{\mathbb{P}}(\beta, E_T^2)] \\ &+ \text{secondary Reggeon contributions.} \end{aligned} \quad (24)$$

The CDF measurements of  $\tilde{F}_{jj}^D$  are shown by the data points in Fig. 3, together with five curves representing predictions of  $\tilde{F}_{jj}^D$  based on various sets of diffractive structure functions, themselves obtained by fitting to HERA diffractive data. The structure functions  $f_i^{\mathbb{P}}(\beta, Q^2)$  are evaluated at  $Q^2 = 75 \text{ GeV}^2$ , which approximately corresponds to the average  $E_T^2$  of the CDF data.

<sup>5</sup> Here we define the Pomeron flux slightly differently to [17] by including  $C_{\mathbb{P}}$  in (22).

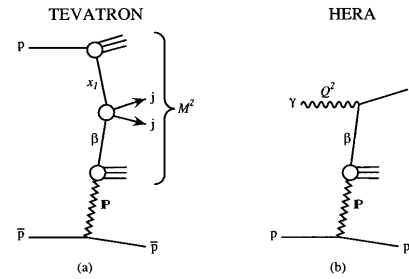


**Fig. 2a,b.** Schematic diagrams for diffractive dijet production at the Tevatron and for diffractive deep inelastic scattering at HERA. The rescattering corrections are omitted in these diagrams

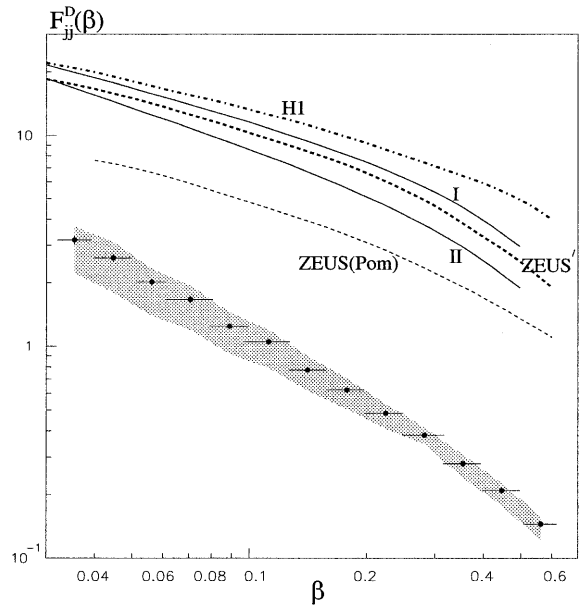


**Fig. 3.** A comparison of the measured CDF dijet diffractive distribution as a function of  $\beta$ , with different predictions obtained from analyses of HERA diffractive data assuming Regge factorization and that rescattering corrections are neglected. The shaded region on the CDF data shows the band of uncertainty shown in [17]

The prediction labelled by H1 is obtained from the H1 diffractive data, and corresponds to fit 2 of the H1 collaboration [22]. The curve labelled by ZEUS(Pom) corresponds to the prediction obtained from ZEUS data in [23]<sup>6</sup>. It does not include the contribution of secondary Reggeons. Note that the ZEUS data are in the region of very small  $\xi$  and thus are practically insensitive to these contributions. The curve labelled ZEUS' includes the secondary Reggeon contribution as determined by H1 collaboration<sup>7</sup>. A comparison of the two latter curves shows

<sup>6</sup> Note that the curve in Fig. 3 for the ZEUS structure function differs from that calculated in [25].

<sup>7</sup> This procedure may not be completely consistent as values of the Pomeron intercept are different in the analyses of the H1 and ZEUS data (see [22,23]). This can lead to a modification of the secondary Reggeon contribution for the ZEUS parametrization.

that the non-Pomeron “background” is rather important in the  $\xi$  region covered by CDF (about 50% of the total contribution). These three predictions are representative of those obtained from the various sets of diffractive structure functions that are available [26]. They illustrate the large uncertainties in the predictions of the shape of  $\tilde{F}_{jj}^D$  at large  $\beta$ , and in the overall normalisation. On the other hand, the shape predicted for  $\beta \lesssim 0.15$  is well determined to be  $\beta^{-\delta}$  with  $\delta = 0.4 - 0.5$ , and differs markedly from the measured  $\delta \simeq 1$  behaviour of the CDF data.

The diffractive gluon distribution is the main contributor to the predictions of  $\tilde{F}_{jj}^D$ . Although the diffractive quark distributions are well-measured at HERA (since the photon couples directly to the quark), the gluon distribution is determined from the detailed  $Q^2$  behaviour of the experimental data using QCD evolution. Moreover, the uncertainties in the diffractive structure functions  $f_i^p(\beta, Q^2)$  are amplified by sizeable differences between H1 and ZEUS diffractive data in certain  $\beta, Q^2$  domains. These uncertainties mainly affect the gluon distribution and are responsible for the ambiguity in the predictions for the shape of  $\tilde{F}_{jj}^D$  at large  $\beta$ , and in the overall normalisation. All the predictions give similar shapes for  $\beta \lesssim 0.15$ , because they are determined mainly by the QCD evolution. We will therefore study this evident difference between the CDF and HERA shape of  $\tilde{F}^D$  at small  $\beta$ , as well as the difference in overall normalisation<sup>8</sup>, which are clearly not reproduced in the naive model based on Fig. 2.

Although we see from the curves shown in Fig. 3 that, at present, there are large uncertainties in the Pomeron structure function measured at HERA, curves I and II should provide a realistic illustration of the range of acceptable values, for the reasons given above. These two alternative curves are used in the analysis of the CDF data presented below. The curve I corresponds to the function  $4.6(1 - \beta)^{1.1}\beta^{-0.45}$ , and is very close to the parametrization of Capella et al. [29] (with secondary reggeons taken from [22]), while the curve II corresponds to the parametrization  $2.5(1 - \beta)\beta^{-0.58}$ , which we choose to account for possible variations due to the uncertainty in the secondary Reggeon contribution. Recall both parametrizations corresponding to  $Q^2 = 75 \text{ GeV}^2$ .

The discrepancies between the Tevatron and HERA data were discussed in [30], where it was emphasized that the survival probability of the gap is (i) small, and (ii) dependent on the value of  $\beta$ . Physical arguments were presented which qualitatively reproduce the scale of normalisation and some trends in the  $\beta$  dependence at large  $\beta$ . Note that the effects causing the observed  $\beta$ -dependence of the diffractive structure function considered in [30] and in this paper concern different regions in  $\beta$  and are of different dynamical origin. While the fall-off at  $\beta \rightarrow 1$

<sup>8</sup> Note that earlier CDF results [27] on diffractive  $W$  boson, dijet,  $b$ -quark and  $J/\psi$  production rates, using forward rapidity gap tagging, have already provided evidence against approaches which do not account for rescattering effects. The observed breakdown of factorization had been foreseen by Goulianos within the so-called renormalized Pomeron flux model [28].

is attributed in [30] dominantly to Sudakov suppression effects, in this paper the variation of the shape of the  $\beta$ -distribution is explained mainly by the competition between the different parton configurations. In this way, we present below a two-channel model prediction, based on [9], which turns out to be in surprising agreement with both the normalisation difference and in the shape of the distributions at low  $\beta$ .

## 5 Diffractive dijet production including rescattering effects

To explain the main features of the CDF diffractive dijet data it is sufficient to consider the two-component diffractive models introduced in Sect. 3. In model A we assume that the sea quarks and gluons mainly occur in large-size configurations of the incident proton, while the valence quarks occupy predominantly small-size configurations. This is, of course, an oversimplification of the real situation, but we find even this simple physical model is able to account for the behaviour of the data.

The two-channel generalisation of (1) gives, using model<sup>9</sup> A of Sect. 3, the survival probability of the gaps<sup>10</sup>

$$|S|^2 = \frac{\int d^2b (|\mathcal{M}_v|^2 e^{-\Omega_v(s,b)} + |\mathcal{M}_{\text{sea}}|^2 e^{-\Omega_{\text{sea}}(s,b)})}{\int d^2b (|\mathcal{M}_v|^2 + |\mathcal{M}_{\text{sea}}|^2)}, \quad (25)$$

where  $\mathcal{M}_{v,\text{sea}}$  are the probability amplitudes (in impact parameter space) of the hard diffractive process corresponding to the valence quark and to the sea quarks and gluons respectively. The functions  $\Omega_i$  can be parametrized in the form<sup>11</sup>

$$\Omega_i = K_i \frac{(g_{pp}^p)^2 (s/s_0)^\Delta}{4\pi B} e^{-b^2/4B}, \quad (26)$$

with  $i = v, \text{sea}$ , and where the slope of the Pomeron amplitude is

$$B = \frac{1}{2}B_0 + \alpha' \ln(s/s_0), \quad (27)$$

with  $s_0 = 1 \text{ GeV}^2$ . We take  $K_v = 1 - \gamma$  and  $K_{\text{sea}} = 1 + \gamma$ , consistent with the simple physical model introduced above. The values of the other parameters were determined in a two-channel global description of the total,

<sup>9</sup> In model B the subscripts ‘v’ and ‘sea’ correspond to the components with the smaller and larger absorption cross sections respectively.

<sup>10</sup> In fact in the calculations a more accurate formula is used which takes into account the inelastic rescatterings of both of the colliding protons, see Appendix B of [9].

<sup>11</sup> We show formula (26) in order to again simplify the discussion. In this simplified form the values of the parameters would be about  $(g_{pp}^p)^2 = 25 \text{ mb}$ ,  $B_0 = 8 \text{ GeV}^{-2}$ ,  $\Delta = 0.1$  and  $\alpha' = 0.15 \text{ GeV}^{-2}$ . However, in practice we use the more realistic  $\Omega_i (i = v, \text{sea})$  that were determined in the global description of total, elastic and soft diffractive data in the ISR to Tevatron energy range [9]. In addition the pion-loop contribution in the Pomeron was included (that is the nearest  $t$ -channel singularity), as well as the contribution coming from large mass single- and double-diffractive dissociation. These refinements are not crucial for the effects that we discuss here.

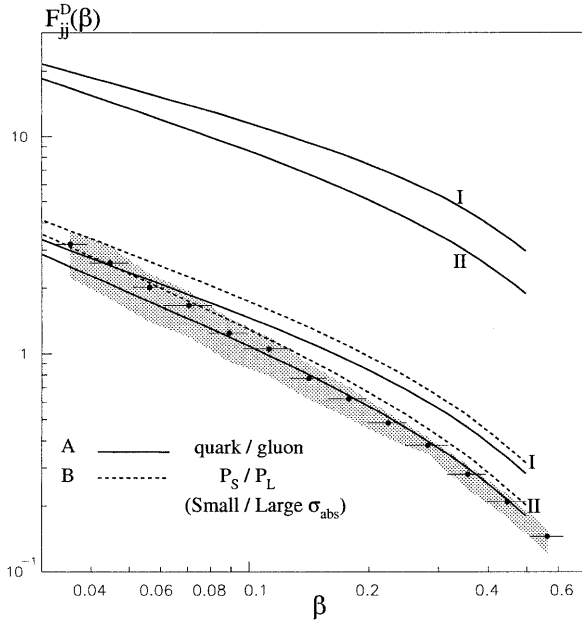


**Fig. 4.** The predictions for diffractive dijet production at the Tevatron, obtained from two alternative sets of ‘HERA’ diffractive parton distributions I and II (of Fig. 3), compared with the CDF data [17]. The upper two curves correspond to the neglect of rescattering corrections, whereas the lower four curves show the effect of including these corrections using model A (continuous curves) and model B (dashed curves) for the diffractive eigenstates ( $|\phi_i\rangle$  of Sects. 2 and 3)

differential elastic and soft diffraction cross sections [9], in which the parameter  $\gamma$  was fixed to be 0.4. Note that in the previous paper [9] both the functions  $\Omega_i$  were required to have a common  $b$  behaviour (in order not to introduce extra parameters). To retain the model we have therefore carried over the same form for both  $\Omega_v$  and  $\Omega_{sea}$ , although, in principle, we might expect them to have a different  $b$  profile.

First we indicate why the soft rescattering effects ( $\Omega_i \neq 0$ ) of the model based on (25) modify the  $\beta$  distribution of the dijet process in a characteristic way. Note that the CDF measurements cover a narrow  $\xi$  interval,  $0.035 \leq \xi \leq 0.095$ , and hence that the invariant mass squared of the diffractively produced state,  $M^2 = \xi s$ , remains close to the average value  $2 \times 10^5 \text{ GeV}^2$ . Also the mass squared of the produced dijet system,

$$M_{jj}^2 = x_1 \beta M^2, \quad (28)$$

see Fig. 2, does not change much compared to its average value of about  $1 \times 10^3 \text{ GeV}^2$  calculated for the CDF kinematical range. Thus  $x_1 \beta \simeq 0.005$  and so for  $\beta \gtrsim 0.25$  we have  $x_1 \lesssim 0.02$ , whereas for  $\beta \sim 0.025$  we have  $x_1 \sim 0.2$ . Therefore for large  $\beta$  (small  $x_1$ ) sea quarks and gluons will give the dominant contribution, while for small  $\beta$  the valence quarks play an important role. Hence the survival probability should increase as  $x_1$  increases and  $\beta$  decreases.

The calculation of the diffraction dijet rate, incorporating the rescattering effects of (25), confirms these expect-

tations, as shown by the lower pair of continuous curves (I and II) in Fig. 4. These curves are parameter-free predictions of the diffractive dijet rate based on the two-channel eikonal model of [9] and on the diffractive distributions obtained from HERA data. The two models (A and B of Sect. 3) for the diffractive eigenstates ( $|\phi_1\rangle$  and  $|\phi_2\rangle$ ) give similar predictions to each other, as shown respectively by the continuous and dashed curves in the lower part of Fig. 3. We see that the pair of curves II satisfactorily reproduce the normalisation and the experimentally observed shape of the  $\beta$  distribution. Curves I also give a satisfactory description at low  $\beta$ ; the difference at larger  $\beta$  just reflects the uncertainty in the ‘HERA’ diffractive distributions. Recall that the predicted shapes show an anomalously strong increase<sup>12</sup>,  $1/\beta^\delta$  with  $\delta \approx 0.8 - 0.9$ , for small  $\beta$ , as compared with the  $\delta \approx 0.4 - 0.5$  behaviour given by the partonic distributions of the Pomeron. A possible change of  $E_T(\text{jet})$ , due to a variation  $\Delta E_T$  of the transverse energy of the underlying event with  $\beta$ , was taken into account in our calculations. We took  $\Delta E_T = C(1 - \beta)^2$  with  $C = 0.76 \text{ GeV}$  chosen so as to satisfy the observed  $\langle \Delta E_T \rangle = 0.54 \text{ GeV}$  [17]. The origin of such  $\beta$ -behaviour can be traced to the fragmentation of the gluon jet. It leads to a small  $\sim 10\%$  decrease of the theoretical predictions for  $\beta \gtrsim 0.2$ .

The overall normalisation of the prediction for the CDF dijet data, which is reproduced by the average value of the survival probability (25), is sensitive to the impact parameter distributions,  $\mathcal{M}_i(s, b)$ , of the hard diffractive process. Such a comparison can therefore provide information on these distributions which, in turn, reveal the spatial structure of the hard process. Our curves are obtained under the same assumptions for the single diffractive production of a massive hadronic state as were used in [9]. That is, as for the minimum bias single diffractive process, but without the term  $\alpha' \ln(M^2/s_0)$ , since  $\alpha' \rightarrow 0$  in (LO) DGLAP evolution to the scale  $\mu^2 \sim 75 \text{ GeV}^2$  of the hard subprocess.

Our calculation of diffractive dijet production illustrates a crucial ingredient necessary in the description of rapidity gap processes. Namely that the survival probability of a gap can depend on  $x_1$  of the partons in the proton (see Fig. 2a). This leads to many experimental consequences for processes with rapidity gaps. For instance, if diffractive dijet production were measured at higher (LHC) energies with the same jet threshold ( $E_T^j$ ), then the values of  $x_1$  of the partons from the proton will be much smaller throughout the same interval of  $\beta$ . Thus the variation of  $|S|^2$  with  $\beta$  will disappear, and the shape of the  $\beta$  distribution in this interval will be close to that measured at HERA. The effect that is observed at the Tevatron is predicted to occur at the LHC, but at much smaller values of  $\beta$ , see (28).

<sup>12</sup> This increase is still somewhat weaker than that seen in the data ( $\delta \approx 1$ ) [17]. However the CDF data include up to 4 jets, while the theoretical predictions are given for 2 jet production. If the data are restricted to two jet production then the increase is less steep (and given by the lower part of the shaded band) [17], and, in fact, in agreement with our  $\beta$  dependence.

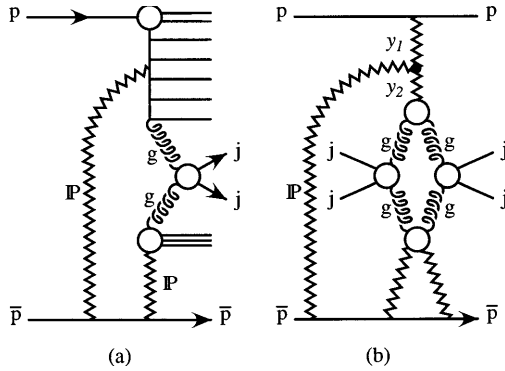


**Fig. 5.** **a** Another possible contribution relevant to the calculation of the survival probability of the rapidity gap in diffractive dijet production, where the ‘rescattering’ Pomeron couples to the upper ‘ladder’, rather than to the incoming proton. **b** The contribution to the diffractive dijet cross section coming from the interference of diagram (a) with the Born diagram of Fig. 2a

### 5.1 Other $\beta$ dependent effects

We also estimated other possible mechanisms that may influence the predictions of the dijet  $\beta$  distribution shown in Fig. 4. We discuss these mechanisms in turn below. None of them is expected to be significant, and anyway influences mainly the region of  $\beta \sim 1$ . Most of the effects tend to make the  $\beta$  distributions steeper and to improve the agreement with experiment. However we have not included them in our predictions so as not to obscure the main phenomenon discussed in our paper.

- (a) The mechanism shown by the diagram of Fig. 5a describes the situation where the Pomeron couples to the ‘ladder’ in the upper part of the diagram, rather than to the proton as we have considered so far. It may influence the value of the survival probability at very small  $x_1$ . The interference of Fig. 5a with the Born diagram of Fig. 2a leads to a contribution to the cross section shown in Fig. 5b. It contributes when the rapidity intervals  $y_i$  (shown in Fig. 5b) are large; note that  $y_1 + y_2 = \ln 1/x_1$ . This effect is small at the Tevatron because of the lack of phase space ( $y_1 + y_2 \lesssim 5$ ), but it should be taken into account at the LHC.
- (b) Another possible non-factorizable contribution is where a soft gluon from the Pomeron couples to the upper partons or spectator quarks of the proton [31, 30]. Their dominant contribution may be summed and absorbed in the regeization of the gluon, that is BFKL effects in parton evolution. The remaining contribution is strongly suppressed since, when the soft  $t$ -channel gluon crosses an  $s$ -channel parton, it changes the colour structure of the corresponding splitting kernel. For the singlet (gluon ladder)  $N_C$  is replaced by  $N_C/2$ , whereas for the non-singlet (quark ladder)  $C_F = (N_C^2 - 1)/2N_C$  is replaced by  $-1/2N_C$ . Using the double log approximation we estimate this effect increases the prediction by less than 10% for small  $\beta$ , and less than 4% for  $\beta > 0.3$ .

- (c) For large  $\beta$  there is an additional Sudakov-like suppression due to QCD radiation from high  $E_T$  jets [30]. Again the dominant contribution is already included in the effective structure of the Pomeron measured in DIS at HERA. However conventional DGLAP evolution does not account for double logs of the type  $(\alpha_S/4\pi) \ln^2(1 - \beta)$ , which sum up to  $\exp(-(\alpha_S/4\pi)C \ln^2(1 - \beta))$ . The effect may be important when  $\beta \rightarrow 1$ , but is negligible in the  $\beta < 0.5$  domain of present interest.
- (d) Hadronization may change the longitudinal momentum of the high  $E_T$  jet [35]. The general effect is to shift the hadronic jet towards the centre-of-mass of the hadronic state,  $M^2$  in Fig. 2a, and to reduce the effective value of  $\beta$ . A conservative estimate is that the prediction for  $\tilde{F}_{jj}^D$  is changed by less than 10% for  $\beta < 0.3$ , although it works in the desired direction to steepen the  $\beta$  dependence.
- (e) The predictions depend on the spatial size of the triple-Pomeron vertex. The corresponding slope  $b_p$  is small, but not well known. We use the same slope  $b_p = 1 \text{ GeV}^{-2}$  as in [9], but  $b_p = 0$  or  $2 \text{ GeV}^{-2}$  are not excluded. Moreover we may expect  $b_p$  to be smaller for larger  $\beta \rightarrow 1$ , when the Pomeron couples just to the hard sub-process. If we take  $b_p = (1 - \beta) \text{ GeV}^{-2}$  then the prediction is unchanged in the small  $\beta$  region, although it decreases by about 10% at  $\beta = 1/3$ . The sensitivity to the radius of the triple-Pomeron vertex indicates the importance of the experimental study of diffractive dissociation processes to better determine  $b_p$ .

## 6 Predictions for other hard diffractive processes

The observation that the suppression factors can depend on the values of the momentum fractions  $x_i$ , carried by the partons in the colliding hadrons, has implications for hard diffractive-like processes in general. For example, diffractive  $W$ -production at the Tevatron [32] is mediated dominantly by valence quarks in the proton, and hence the survival probability for such a process is comparatively large,  $S^2 \simeq 0.2 - 0.3$ . On the other hand, for diffractive processes mediated by the gluonic components of the colliding hadrons (such as  $b\bar{b}$ ,  $J/\psi$ ,  $\psi'$  or  $\Upsilon$  production) the survival probabilities should be smaller  $S^2 \simeq 0.06 - 0.1$ .

An interesting application is to the production of two high  $p_T$  jets ( $\mathbf{p}_{1T} \simeq -\mathbf{p}_{2T}$ ) separated by a large rapidity gap, as measured by both the D0 [33] and CDF [34] collaborations at the Tevatron at two energies,  $\sqrt{s} = 630$  and  $1800 \text{ GeV}$ . Both the quark and gluon components of the proton contribute in this case. However, in our approach the suppression factor depends strongly on the type of parton (model A) or on the  $x$  value of the parton (model B). For a fixed energy  $\sqrt{s}$ , the ratio of the quark to the gluon component increases as  $E_T$  of the jets increases, and as the rapidity interval  $\Delta\eta$  between the jets increases. The relative importance of the quark component also increases as

the energy  $\sqrt{s}$  decreases, simply due to kinematics. These features of the simple two-channel model give effects which move in the right direction to explain outstanding puzzles in the interpretation of the D0 and CDF data for jets separated by a rapidity gap [33,34]. In particular, they help to understand the  $\sqrt{s}$ ,  $E_T$  and  $\Delta\eta$  dependences of the colour-singlet (rapidity gap) fraction measured at the Tevatron [33,34]. Our model gives a natural explanation of the observation by the D0 collaboration, that the suppression factor depends mainly on the  $x$  of the partons such that the cross section increases strongly with  $x$ , see Fig. 4d of [33].

All of the effects discussed above can be studied in hard diffractive processes in  $p$ -nucleus collisions at RHIC and LHC. Investigation of the  $A$ -dependence can provide new information on the strength of shadowing effects. Indeed for weak shadowing, the cross sections for *coherent* diffraction dissociation of a proton on nuclei behave as  $\sim A^{4/3}$ , while *incoherent* diffraction cross sections behave as  $\sim A$ . In the opposite limit of very strong shadowing both cross sections have much weaker dependence on  $A$ , of the form  $\sim A^{1/3}$ . Thus there is a strong change in  $A$ -dependence of diffractive production on nuclei depending on the strength of the shadowing effects.

We also note that the survival probability for central Higgs production by  $WW$  fusion, with large rapidity gaps on either side, is enhanced in the two-channel model in comparison with previous estimates [9,11], which also included allowance for the survival probability. Thus in [9] for  $WW \rightarrow H$  process at the LHC  $S^2$  was found to be 0.15, while the approach of this paper gives  $S^2 = 0.24$ . This is an important process because it appears that large  $q_T$  Higgs configurations can be chosen such as to identify the Higgs over the possible background processes at the LHC [37,36]. The same survival probability is applicable to central  $Z$  boson production with a rapidity gap on either side, originating from  $t$ -channel gauge boson exchange. Therefore  $Z$  production at the LHC can be used to directly measure the survival probability of rapidity gaps relevant to Higgs production by  $WW$  fusion [3].

## 7 Conclusions

For hard processes with large rapidity gaps, we have demonstrated that the survival probability of the gaps has a much richer structure than is given by the simple one-channel eikonal approximation of (1). We introduced two-channel eikonal models in which *either* the valence quark and the sea quark (+ gluon) components of the proton have substantially different total cross sections of absorption  $\sigma_i^{\text{tot}}(s)$ , which we called model A, *or* alternatively, model B, in which the small and large size diffractive components are specified according to sum rules (17) and (18). The two models give similar results, and predict that the survival probability of the rapidity gap has a characteristic dependence on the kinematics of the process. Data for diffractive dijet production at the Tevatron [17] enabled this kinematic dependence to be checked. Taking the parameters of the two-channel models which were previously

constrained in a global description [9] of total, elastic and soft diffraction data, we calculated the  $\beta$  distribution of diffractive dijet production. The results are shown by the lower four curves in Fig. 4. We see that there is general agreement between the predictions and the CDF measurements [17], both in normalisation and shape. In fact, the use of Pomeron structure function II quantitatively reproduces the CDF data [17]. We emphasize that if the Pomeron structure function were known unambiguously then we would have an essentially unique prediction for the Tevatron data, demonstrated by the small difference between the predictions of models A and B.

Unfortunately, the agreement between the CDF diffractive dijet data and our calculations can be taken as a strong support for the low value of the survival probability  $S^2$ , which leads to the rather pessimistic expectations for the missing-mass Higgs search at the Tevatron [6,38].

As precise data for other hard processes with rapidity gaps become available, it will be possible to refine the model and to identify the parton content of the diffractive eigenchannels. We already showed that the simple two-channel model gave rescattering corrections which moved in the right direction to resolve discrepancies between the predictions and the data for processes which have so far been measured. In this way, as precise data become available, it will be possible to perform a quantitative study to (i) determine the partonic content of the Pomeron, (ii) check the QCD evolution of the Pomeron structure functions, (iii) confirm the universality of the partonic decomposition, (iv) determine  $\sigma_i^{\text{tot}}(s)$  for the different diffractive eigenchannels, and (v) measure the impact parameter distributions of the ‘Born’ amplitudes of the hard processes with rapidity gaps.

*Acknowledgements.* We thank Dino Goulianos and Ken-ichi Hatakeyama for useful discussions. One of us (VAK) thanks the Leverhulme Trust for a Fellowship. ABK and MGR would like to thank the IPPP of the University of Durham for hospitality. This work was partially supported by the UK Particle Physics and Astronomy Research Council, the EU Framework TMR programme, contract FMRX-CT98-0194 (DG 12-MIHT), NATO grant PSTCLG-977275 and also by grants RFBR 00-15-96610, 00-15-96786, 01-02-17095 and 01-02-17383.

## References

1. Yu.L. Dokshitzer, V.A. Khoze, T. Sjöstrand, Phys. Lett. **B274**, 116 (1992)
2. J.D. Bjorken, Int. J. Mod. Phys. **A7**, 4189 (1992); Phys. Rev. **D47**, 101 (1993)
3. H. Chehime, D. Zeppenfeld, Phys. Rev. **D47**, 3898 (1993)
4. R.S. Fletcher, T. Stelzer, Phys. Rev. **D48**, 5162 (1993)
5. E.M. Levin, hep-ph/9912402 and references therein
6. V.A. Khoze, A.D. Martin, M.G. Ryskin, Eur. Phys. J. **C19**, 477 (2001) and references therein
7. M.M. Block, F. Halzen, Phys. Rev. **D63**, 114004 (2001)
8. M.G. Albrow, A. Rostovtsev, hep-ph/0009336 and references therein
9. V.A. Khoze, A.D. Martin, M.G. Ryskin, Eur. Phys. J. **C18**, 167 (2000)



10. V.A. Khoze, A.D. Martin, M.G. Ryskin, Nucl. Phys. Proc. Suppl. **99**, 525 (2001)
11. V.A. Khoze, A.D. Martin, M.G. Ryskin, Eur. Phys. J. **C14**, 525 (2000)
12. E. Gotsman, E. Levin, U. Maor, Phys. Lett. **B452**, 387 (1999); Phys. Rev. **D60**, 094011 (1999)
13. A.B. Kaidalov, Phys. Rep. **50**, 157 (1979)
14. J. Pumplin, Physica Scripta **25**, 191 (1982)
15. M.L. Good, W.D. Walker, Phys. Rev. **126**, 1857 (1960)
16. V.N. Gribov, Sov. Phys. JETP **19**, 483 (1969)
17. CDF Collaboration: T. Affolder et al., Phys. Rev. Lett. **84**, 5043 (2000)
18. K.G. Boreskov, A.M. Lapidus, S.T. Sukhorukov, K.A. Ter-Martirosyan, Nucl. Phys. **B40**, 397 (1972)
19. L. Van Hove, K. Fialkowski, Nucl. Phys. **B107**, 211 (1976)
20. H.I. Miettinen, J. Pumplin, Phys. Rev. **D18**, 1696 (1978)
21. A.B. Zamolodchikov, B.Z. Kopeliovich, L.I. Lapidus, JETP Lett. **33**, 595 (1981); G. Bertsch, S.J. Brodsky, A.S. Goldhaber, J.F. Gunion, Phys. Rev. Lett. **47**, 297 (1981)
22. H1 Collaboration: T. Ahmed et al., Phys. Lett. **B348**, 681 (1995); C. Adloff et al., Z. Phys. **C76**, 613 (1997)
23. ZEUS Collaboration: M. Derrick et al., Z. Phys. **C68**, 569 (1995); Phys. Lett. **B356**, 129 (1995); Eur. Phys. J. **C6**, 43 (1999)
24. G. Ingelman, P. Schlein, Phys. Lett. **B152**, 256 (1985)
25. C. Royon, L. Schoeffel, J. Bartels, H. Jung, R. Peschanski, Phys. Rev. **63**, 074004 (2001)
26. K.J. Golec-Biernat, J. Kwiecinski, Phys. Lett. **B353**, 329 (1995); T. Gehrmann, W.J. Stirling, Z. Phys. **C70**, 227 (1995)
27. See K. Goulianos, Nucl. Phys. Proc. Suppl. **99**, 37 (2001), for a recent review
28. K. Goulianos, preprint Fermilab-conf-99/154-E; J. Phys. **G26**, 716 (2000), and references therein
29. A. Capella, A. Kaidalov, C. Merino, D. Pertermann, J. Tran Thanh Van, Phys. Rev. **D53**, 2309 (1996)
30. V.A. Khoze, A.D. Martin, M.G. Ryskin, Phys. Lett. **B502**, 87 (2001)
31. J.C. Collins, L. Frankfurt, M. Strikman, Phys. Lett. **B307**, 161 (1993)
32. CDF Collaboration: F. Abe et al., Phys. Rev. Lett. **79**, 2636 (1997)
33. D0 Collaboration: B. Abbott et al., Phys. Lett. **B440**, 189 (1998)
34. CDF Collaboration: F. Abe et al., Phys. Rev. Lett. **80**, 1156 (1998); **81**, 5278 (1998)
35. B. Cox, J.R. Forshaw, L. Lönnblad, hep-ph/9912489
36. V.A. Khoze, A.D. Martin, M.G. Ryskin, hep-ph/0104230, Eur. Phys. J. C. (in press)
37. N. Kauer, T. Plehn, D. Rainwater, D. Zeppenfeld, Phys. Lett. **B503**, 113 (2001)
38. V.A. Khoze, A.D. Martin, M.G. Ryskin, hep-ph/0103007